Accepted: 20 March 2023 / DOI: 10.1109/TNS.2023.3262409

Amplitude Measurements with SiPM and ASIC (Citiroc 1A) Front-End Electronics

M. Perri, P. Garosi, C. Mattone, C. Tintori, M. Corbo, D. Ninci, M. Venaruzzo, Y. Venturini, A. Saltarelli

***Abstract*—The use of Application Specific Integrated Circuits (ASICs) in nuclear physics instrumentation is drastically increasing, thanks to the possibility of incorporating a large number of acquisition channels in compact devices. In this paper, we describe a SiPM-based application with CAEN Front-End Readout System [1] based on Citiroc 1A chip from Weeroc [2]. Besides the use of this chip for well known single photon spectra and event counting, this paper exploits the possibility to acquire energy spectra directly from scintillators, paired with SiPM, through peak-and-hold readout. In particular, good energy resolutions have been achieved even with slow scintillators, like LYSO, CsI(Tl), and BGO, which have 40 ns, 1000 ns, and 300 ns of light decay time, respectively. These values are of the same order of magnitude of the shaping time of the Citiroc 1A chip (maximum value of 87.5 ns) in the case of LYSO, and higher in the case of CsI(Tl) and BGO. Several measurements have been performed using multiple radioactive γ sources and the resulting energy spectra demonstrate a resolution compatible with that found in literature [4] [5] [6] [7], as well as with an alternative acquisition system based on a digitizer that implements an algorithm of Charge Integration in the FPGA [8].**

***Index Terms*—Gamma Spectroscopy, Citiroc 1A, ASIC, FERS-5200, MPPC, SiPM.**

I. Introduction

The study of nuclear physics and its several applications in industry, medicine, academic, and applied research, demands for new setup capable of managing an ever more increasing number of readout channels. Application Specific Integrated Circuit (ASIC) is a promising candidate to satisfy this demand, since it gives the possibility of integrating complex circuits in a reduced space with small power consumption.

In this paper, we made use of CAEN A5202 FERS-5200 board [1], which integrates two Citiroc 1A ASIC chips from Weeroc [2]. This board was selected for its high number of channels (sixty-four channels, thirty-two channels per chip) easily scalable to hundreds of channels, and for the flexibility of multiple communication infrastructures and convenient sensors connection.

The Citiroc 1A chip has already been extensively characterized by measuring the trigger efficiency and linearity, response to temperature and optical cross talk [9]. Its robustness and flexibility make the Citiroc 1A suitable for a large number of applications, from cosmic ray measurements [10], anti-coincidence gamma measurements for astrophysics [11], X and γ-rays detectors for space mission [12], medicine applications as Wearable Positron Emission Tomography [13], and applications for Pulse Shape Discrimination (PSD) in high-density channel Imager [14].

Preliminary results obtained with the A5202 board are based on single photon sensitivity and counting capability of the system, like in the case of high granular calorimetry for high energy physics and multi-channel dosimetry for brachytherapy [15], as well as radioactive waste monitoring applications [16]. Characterization and preliminary cosmic rays measurements are reported in [1] and [17], respectively.

This paper explores the possibility to use the Citiroc 1A chip to acquire γ energy spectra from slow scintillator detectors, where the light decay time is comparable or even higher than the shaping time of the chip. In particular, we used LYSO, Caesium Iodine (CsI(Tl)), and Bismuth Germanate (BGO) crystals which have a decay time of 40 ns, 1000 ns, and 300 ns, respectively.

Citiroc 1A has a maximum shaping time of 87.5 ns, which in principle could be enough just for the LYSO detector; anyway, good resolutions are achieved for all the three detectors. We obtained energy spectra from three γ radioactive sources (^{22}Na, ^{60}Co, and ^{137}Cs) with resolutions compatible with expectations from literature [4] [5] [6] [7] and from a complementary system [8] which uses a digitizer with charge integration algorithm as acquisition system.

ASIC chips with higher shaping time than Citiroc 1A [7] and different pulse processing [18] were already successfully used for γ spectroscopy. This is the first time that Citiroc 1A chip is used for γ spectroscopy measurements and scintillators with slow light decay time.

II. Front-End Electronic Structure

The A5202 board (see Fig. 1) is an all-in-one SiPM readout system which integrates two Citiroc 1A chips (petrol green boxes in the figure) for a total of sixty-four acquisition channels, a power supply module for the SiPM bias (green box), an

Manuscript received 22 August 2022; revised 1 March 2023

Marco Perri is with the department of physics of Camerino (MC) - Italy and collaborating with CAEN S.p.A. in Viareggio (LU) - Italy for his PhD project, as well as with the I.N.F.N. - section of Perugia (e-mail: marco.perri@unicam.it).

Paola Garosi is with CAEN S.p.A. in Viareggio (LU) - Italy (e-mail p.garosi@caen.it)

Cristina Mattone is with CAEN S.p.A. in Viareggio (LU) - Italy (e-mail c.mattone@caen.it)

Carlo Tintori is with CAEN S.p.A. in Viareggio (LU) - Italy (e-mail c.tintori@caen.it)

Matteo Corbo is with CAEN S.p.A. in Viareggio (LU) - Italy (e-mail m.corbo@caen.it)

Daniele Ninci is with CAEN S.p.A. in Viareggio (LU) - Italy (e-mail d.ninci@caen.it)

Massimo Venaruzzo is with CAEN S.p.A. in Viareggio (LU) - Italy (e-mail m.venaruzzo@caen.it)

Yuri Venturini is with CAEN S.p.A. in Viareggio (LU) - Italy (e-mail y.venturini@caen.it)

Alessandro Saltarelli is with the department of physics of Camerino (MC) - Italy, as well as with the I.N.F.N. - section of Perugia (e-mail: alessandro.saltarelli@unicam.it.)

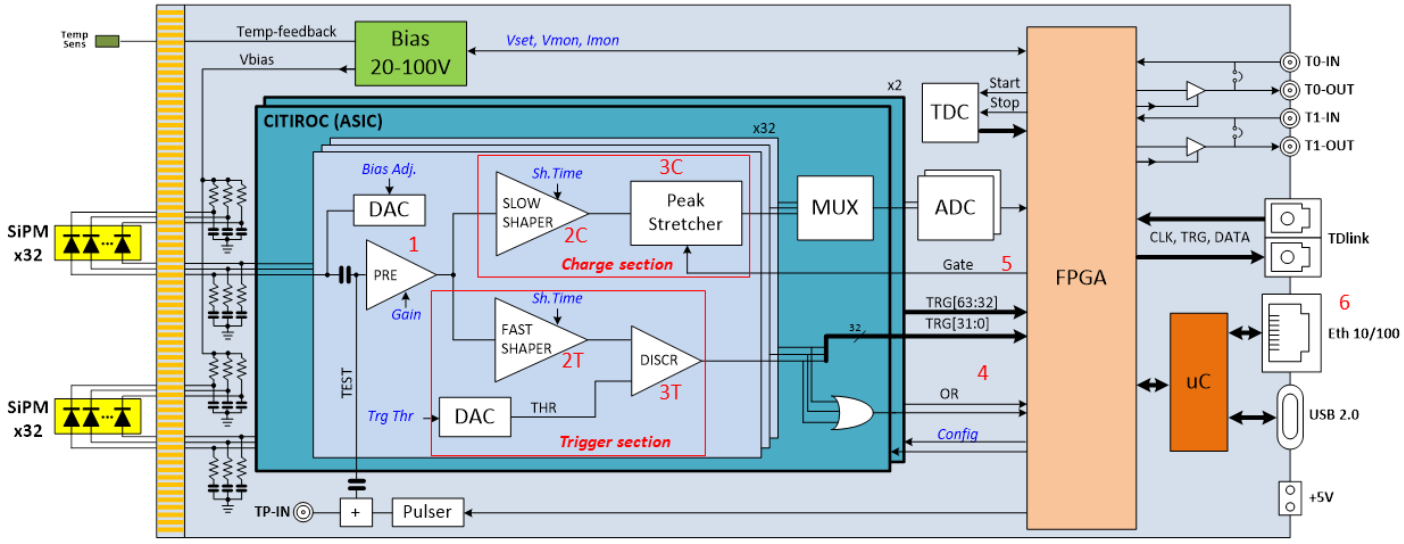

Fig. 1. Scheme of A5202 board, which contains two Citiroc 1A chips (petrol green boxes), the SiPM power supply (green box), the FPGA (light orange box), the communication interfaces, and general purpose I/Os. More details are reported in the text.

FPGA (light orange box), multiple communication interfaces (USB, Ethernet, and optical link), and general purpose I/Os.

The bias for the SiPM is provided through an integrated power supply module and it can be finely tuned channel by channel through an individual DAC in the Citiroc 1A. A temperature feedback circuit is also available to compensate temperature variations. Our measurements were taken at room temperature.

The Citiroc 1A chip is made of a preamplifier ("1" in the figure) and two circuits, one for the charge measurement ("Charge section" in the figure) and one for the time measurement ("Trigger section" in the figure). Two preamplification stages can be chosen in the preamplifier, one with high gain (HG) and the other with a lower gain (LG), in order to cover as much as possible the dynamic range of the pulse. Every channel preamplifier can be shut down to disconnect eventually noisy channels.

The trigger section is composed by a fast shaper (2T) of 15 ns non programmable peaking time and a discriminator (3T), whose output is sent to the FPGA of the A5202 board. The trigger of the single channels and the logic OR combination line (4) can be propagated to the FPGA. An additional discriminator is available in the chip, but not used in this paper.

The charge measurement section is made by a slow CR-RC^2 shaper (2C) and a peak-and-hold circuit (3C). The shaping time of 2C can be tuned from a minimum of 12.5 ns to a maximum of 87.5 ns with a pitch of 12.5 ns, common to all the channels, but can be differentiated between the low gain portion and the high gain portion of the Citiroc 1A.

Fig. 2 shows a scheme of the peak sensing functioning. The peak stretcher, marked 3C in Fig. 1, works in three sequential phases: before the trigger arrival, the peak sensing is turned off (OFF phase); upon the arrival of the trigger from the FPGA (5), the peak detector switches on and memorizes the maximum of the input signal and this phase is held until a rising edge of the hold signal is sensed (Peak Sensing phase); finally, the slow shaper is disconnected to ensure that no other value is memorized (Hold phase). Hold phase is used during the serial read-out of the ASIC. The time window between the trigger and the hold phase is called "Hold Delay"; this is a programmable value which has been optimized in Sec. IV.

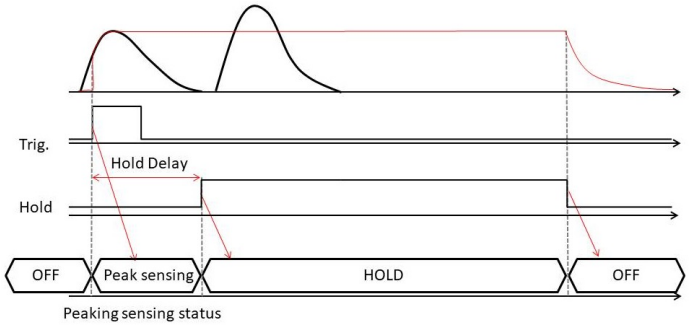

Fig. 2. Citiroc 1A peak sensing working principle. Once the trigger signal is issued, the system switches to the peak sensing phase and finds the peak on the incoming pulse. Upon the arrival of the hold signal the system goes to the "hold" phase in which it disconnects to the shaper to avoid any other pulse entering the system and invalidate the measure. At the arrival of the hold signal falling edge, the "OFF" phase starts and the cycle begins again upon the arrival of a new trigger.

The A5202 can operate in four different modes: spectroscopy (SM), counting (CM), timing (TM), and spectroscopy plus timing (STM) mode. In SM, which is used in this paper, a global (bunch) trigger, either coming from an external source or generated by a combination of the channel self-triggers, starts the peak sensing and creates a data packet containing the common trigger time stamp followed by the individual energies. The packet is saved into the local memory buffer of the A5202 unit, waiting for the readout, while a new cycle can start. In SM, the A/D conversion causes a systematic dead time of about 10 μs, thus limiting the maximum trigger rate to about 100 kcps. In CM all the channels self trigger and they are individually counted in a time interval with a maximum

counting rate of about 20 Mcps. Finally in TM a list of all the individual events time stamps with LSB time resolution of 500 ps is generated by means of a common start or stop signal; the time over threshold is also available for a rough estimation of the pulse amplitude. In STM, both the SM and TM are applied simultaneously and the energy and timing information is available for each bunch trigger.

The available communication interfaces are a USB 2.0, an Ethernet 10/100T, and an optical link (TDLink); for the current measurement, we used the Ethernet connection. I/Os can be programmed to show monitoring signals from chip or FPGA, as shown for example in Fig. 4, and to propagate the trigger and other signals.

III. Experimental Setup

Measurements with two types of experimental setups were performed. The first one was used to verify the possibility to get energy spectra in case of a SiPM coupled with a single crystal (I). The second setup (II) used a different hardware and was made to verify the consistency of results obtained with I. The two setups are described in details below.

In I, we used three different scintillator crystals from Hilger Crystals LTD, in particular CsI(Tl), LYSO, and BGO [22] of $6 \times 6 \times 15$ mm^3 coupled with optical grease with three Hamamatsu SiPM MPPC S13360-6050CS [3]. The SiPM was a single channel with effective photosensitive area of 6×6 mm^2 and a pixel size of 50 μm. Operating voltage was set to 53.8 V and the measurements were performed at room temperature. Each detector and SiPM was connected to the A5202 through the A5253 adapter [21]. We acquired one channel at a time to build the energy spectra from three radioactive sources: ^{22}Na, ^{137}Cs, and ^{60}Co with activities of about 87, 7, and 12 kBq, respectively. A picture of the first experimental setup is shown in the top panel of Fig. 3. On the bottom panel of the figure, a single SiPM and LYSO detector are labelled as (A) and (B), respectively. The acquisition settings, the spectra plot, and data saving were controlled by the CAEN Janus software [23].

In II, we used the CAEN SP5600 amplification unit [24] and DT5720A desktop digitizer [8]. The SP5600 can power supply the SiPM and can provide the preamplification stage. The DT5720A is a waveform digitizer which samples the signal coming from the preamplifier with 4 ns sampling time and 12 bit ADC, and converts it into a digital signal. The internal FPGA of DT5720A calculates the input baseline and triggers the event when the samples cross a programmable threshold with respect to the baseline. For each event passing the selection, a digital gate is opened: baseline subtracted samples are summed together in the time window of the gate and the resulting value is used to fill the energy histogram. This algorithm is called Charge Integration [25]. This system is more suitable for processing signals with longer decay time, like those from CsI(Tl) and BGO, since the integration can cover the entire tail of the pulses.

We decided to use this alternative setup and repeat the same measurements as in I with the same SiPMs and detectors to have reference measurements and be able to make one-to-one comparisons with II. The resolutions reported in [4], [5], [6], and [7] were obtained with crystals of different dimensions than the ones we used, so it is difficult to consistently compare their results with what we obtained.

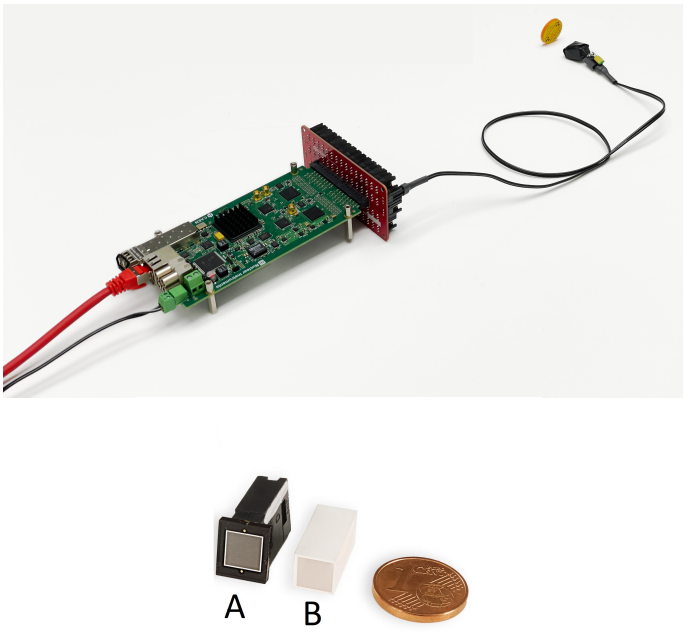

Fig. 3. On the top, a picture showing the setup I, where the A5202 board is connected through the A5253 adapter to a single SiPM coupled with a LYSO crystal, and a ^{22}Na radioactive source. The detector and SiPM were placed in a dark environment, not shown in the picture. On the bottom panel: (A) is the 6×6 mm^2 SiPM used in the setups, and (B) is the single LYSO detector. Finally, the coin is a one euro cent coin we added in the picture as a reference scale.

IV. Event Selection

To acquire events from A5202, we first verified that the events are correctly processed by the Citiroc 1A. In particular, the chip provides some monitoring signals, like the output of the slow shaper (2C), and the output of the preamplifier (1), that can be propagated to one of the output connectors of the A5202 and shown in an oscilloscope. Fig. 4 shows on top the output of the trigger discriminator (3T) in blue and the output of the slow shaper in red. The shape of this pulse depends on the value of the shaping time (87.5 ns in this case): the positive component of the red pulse is the same for all the crystals, while the pole-zero compensation varies according to the tail of the input pulse. The bipolar shape is expected from the Citiroc 1A circuitry, but only the positive part is taken into account for the energy calculation.

We performed a scan of the available shaping time values to verify the best value. Considering the decay time of the three crystals, 40 ns for LYSO, 300 ns for BGO, and 1000 ns for CsI(Tl), and that the shaping of Citiroc 1A goes from 12.5 ns to 87.5 ns, we expected to have the best results using the maximum shaping time of 87.5 ns. We collected the ^{22}Na energy spectrum using the LYSO detector for each of the values of shaping time allowed. The spectra seems to shift

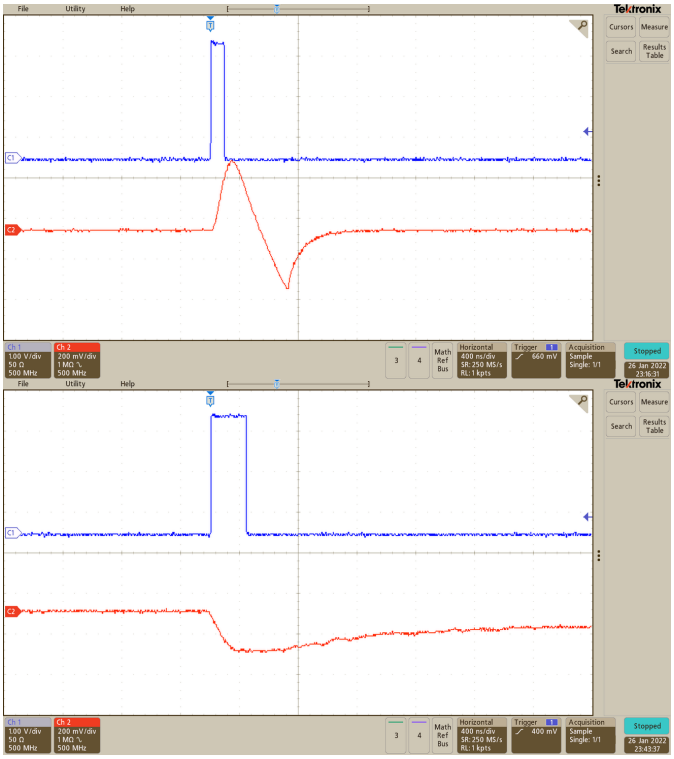

Fig. 4. On the top panel, in blue the output of the trigger discriminator and in red the output of the slow shaper in case of the LYSO detector when the shaping time is set to 87.5 ns. The positive component of the red pulse is the same for all the crystals, while the pole-zero compensation varies according to the tail of the input pulse. On the bottom panel, the red pulse is the output of the preamplifier with the CsI(Tl) detector.

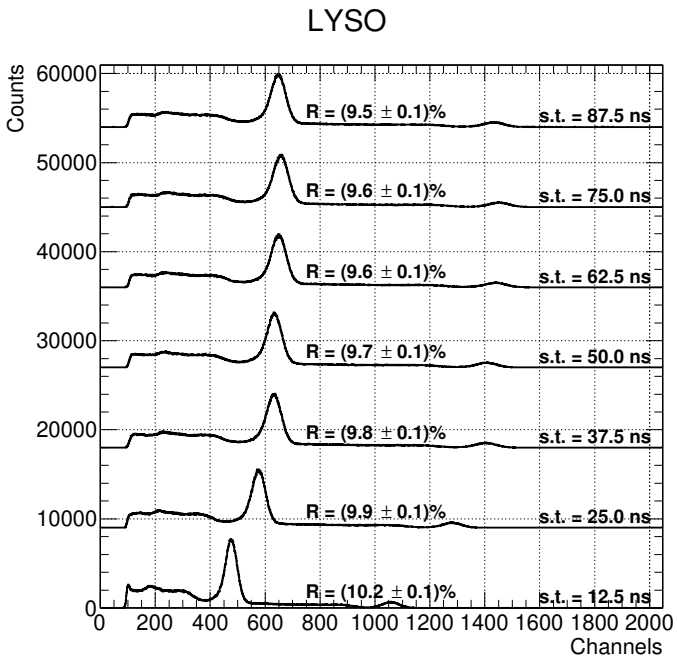

Fig. 5. ^{22}Na energy spectra acquired with the LYSO detector by varying the shaping time (s.t. in the figure). The resolution R = FWHM/Peak of the 511 keV peak is reported for each spectrum. The spectra acquired with smaller shaping time are shifted to the left respect to the ones obtain with shaping time of 50 ns or higher. This effect is caused by a decrease in charge collection resulting from using a smaller shaping time, consequently producing an output signal with smaller amplitude. When utilizing shaping times less than 40 ns, the system collects only a portion of the signal generated by the LYSO crystal.

to the right as the shaping time is increased. This effect is caused by a reduction in charge collection when using smaller shaping time. Since the light decay time of the LYSO crystal is 40 ns, for smaller shaping times the slow shaper collects only a portion of the signal and, as a consequence, the shaper output amplitude is smaller. The spectra are reported in Fig. 5 together with the resolution (R) of the 511 keV annihilation peak. The resolution is defined as the Full Width Half Maximum of the peak, FWHM, over the peak mean value, obtained by means of a Gaussian fit of the peak with a polynomial function for the background. For values higher than 50 ns (i.e. higher than the 40 ns decay time of LYSO), the resolution at 511 keV stabilizes at around 9.5-9.6%.

Considering that the other crystals have higher decay time and that the resolution has its best value at 87.5 ns, we decided to use this value also for CsI(Tl) and BGO without making further scans. Though only a portion of the pulse is expected to be sensed, this portion is proportional to the entire pulse energy.

The last setting we optimized is the “hold delay”, defined as the time difference between the trigger and the arrival of the hold signal (see Fig. 2). The peak of the slow shaper output should arrive within this time interval, to have its maximum correctly evaluated. If the hold signal arrives too early, the peak sensing takes as the maximum just a portion of the pulse, thus giving incorrect results. To optimize this parameter, we acquired again the energy spectrum of the ^{22}Na with the LYSO crystal and a single 6×6 mm^2 SiPM. We fixed the shaping time to the optimized value of 87.5 ns and we varied the hold delay from 50 ns to 350 ns. We evaluated the position of the 511 keV peak for each spectrum and we reported this value of channels versus the hold delay in Fig. 6.

The peak position stabilizes approximately after a value of 200 ns of the hold delay, thus indicating that after 200 ns the peak sensing is able to correctly evaluate the maximum height of the pulse, while for values below 200 ns, the energy is underestimated. For the measurements described in this paper, we used the value of 300 ns.

V. Results

Results from I and II show the typical energy spectra for the three γ radioactive sources used for this paper, ^{22}Na, ^{137}Cs, and ^{60}Co. Fig. 7 and Fig. 8 report the spectra made with the LYSO, CsI(Tl), and BGO detectors (from top to bottom) and ^{22}Na, ^{137}Cs, and ^{60}Co sources (from left to right) acquired with I and II, respectively. All spectra are calibrated in enegy in order to convert channels into keV.

On Table I, the resolutions and the statistical uncertainties of the four peaks (511 keV of ^{22}Na, 662 keV of ^{137}Cs, 1172, and 1332 keV of ^{60}Co) were reported for setup I and II for a quick comparison. The resolutions were obtained through Gaussian fits of the peaks, with polynomial function for background subtraction. Corrections for the SiPM saturation are not taken into account since this contribution will cancel

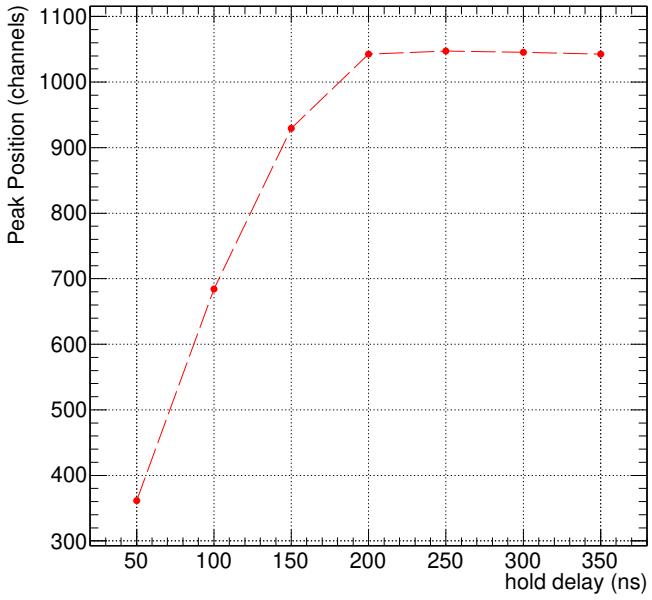

Fig. 6. Position of the ^{22}Na annihilation peak as a function of the hold delay parameter. The measurements have been performed with the LYSO crystal. For values smaller than 200 ns, the peak detection system only sees a portion of the rising time of the slow shaper output and it does not find the correct maximum. After 200 ns, the system evaluates the correct maximum value and the ^{22}Na peak gets stabilized.

out in the comparison between I and II. Anyway, considering the linearity curve calculated from [26], the SiPM saturation will affect mostly the peaks of the ^{60}Co which have higher energy, while below those values, the SiPM is in the linear region.

TABLE I
RESOLUTIONS OBTAINED WITH A5202 FERS-5200 BOARD (SETUP I) AND WITH THE DT5720A DESKTOP DIGITIZER (SETUP II). THE RESOLUTIONS HAVE BEEN CALCULATED AS THE FWHM OVER THE PEAK CENTER (R = FWHM/PEAK), BACKGROUND SUBTRACTED.

	^{22}Na (511 KeV)	^{137}Cs (662 KeV)
A5202+LYSO (I)	(9.5 ± 0.1)%	(9.3 ± 0.1)%
DT5720A+LYSO (II)	(12.3 ± 0.1)%	(10.3 ± 0.1)%
A5202+CsI(Tl) (I)	(11.9 ± 0.1)%	(10.9 ± 0.1)%
DT5720A+CsI(Tl) (II)	(9.6 ± 0.1)%	(8.9 ± 0.1) %
A5202+BGO (I)	(14.4 ± 0.1)%	(13.5 ± 0.1)%
DT5720A+BGO (II)	(12.0 ± 0.1)%	(11.0 ± 0.1)%
	^{60}Co (1172 KeV)	^{60}Co (1332 KeV)
A5202+LYSO (I)	(5.8 ± 0.1)%	(5.0 ± 0.1)%
DT5720A+LYSO (II)	(6.3 ± 0.4)%	(5.4 ± 0.2)%
A5202+CsI(Tl) (I)	(5.8 ± 0.2)%	(5.6 ± 0.1)%
DT5720A+CsI(Tl) (II)	(5.6 ± 0.2)%	(5.4 ± 0.1)%
A5202+BGO (I)	(8.7 ± 0.1)%	(7.1 ± 0.1)%
DT5720A+BGO (II)	(7.7 ± 0.3)%	(6.8 ± 0.4)%

VI. CONCLUSIONS AND DISCUSSION

Comparing the results reported in Table I and the plots of Figs. 7 and 8 between I and II, we found that compatible results were obtained for the two systems.

The LYSO crystal has its own γ radioactivity, which causes a prominent background in the energy region of the 662 keV peak of ^{137}Cs (2 in Figs. 7 and 8). By making a background subtraction of the LYSO radioactivity spectrum, the ^{137}Cs spectrum (2) will result very similar to spectra 5 and 8. This effect is not visible for the ^{22}Na source, despite the 511 keV annihilation peak being close to the LYSO energy emission, because the source activity was high enough to overcome the background. Compton background is prominent especially in the case of CsI(Tl) crystal (plots 4, 5, and 6), due to the reduced dimensions of the crystals; anyway the characteristic peaks are clearly visible for all the sources and for all the detectors.

In the case of LYSO (plot 1, 2, and 3 of Figs. 7 and 8), the resolution obtained with I is better by about 20-30% rather than what achieved with the more traditional acquisition system II.

In the case of CsI(Tl) and BGO detectors, measurements from II and from literature [6] [4][1] are better than what obtained with I by a factor of about 20%, though of the same order for ^{60}Co source, due to the poor resolution of the peaks themselves, which are not well separated. As expected, the limitation comes from the maximum shaping time of 87.5 ns, too short to get the full amplitude of CsI(Tl) and BGO, which is instead well integrated with the charge integration algorithm. Saturation effects also limit the resolution and separation of the ^{60}Co peaks.

In this paper, we successfully explored the possibility to perform nuclear spectroscopy measurements using scintillator detectors paired with SiPM, acquiring radiation coming from three different γ sources with the Citiroc 1A chip integrated in the A5202 board. The system used in this paper has good performances especially with fast scintillating detectors, like LYSO, and have resolution of the same order with slower detectors, like CsI(Tl) and BGO, which makes the A5202 a good candidate for SiPM-based gamma spectroscopy applications requiring high channel density.
Future measurements can exploit the performances of this readout system in conjunction with crystals with faster decay time, like $LaBr_3$ or $CeBr_3$, and bigger dimensions.

[1]Resolution reported in the references for the 511 ^{22}Na peak are around 11%, 10 %, and 12% for LYSO, CsI(Tl), and BGO, respectively

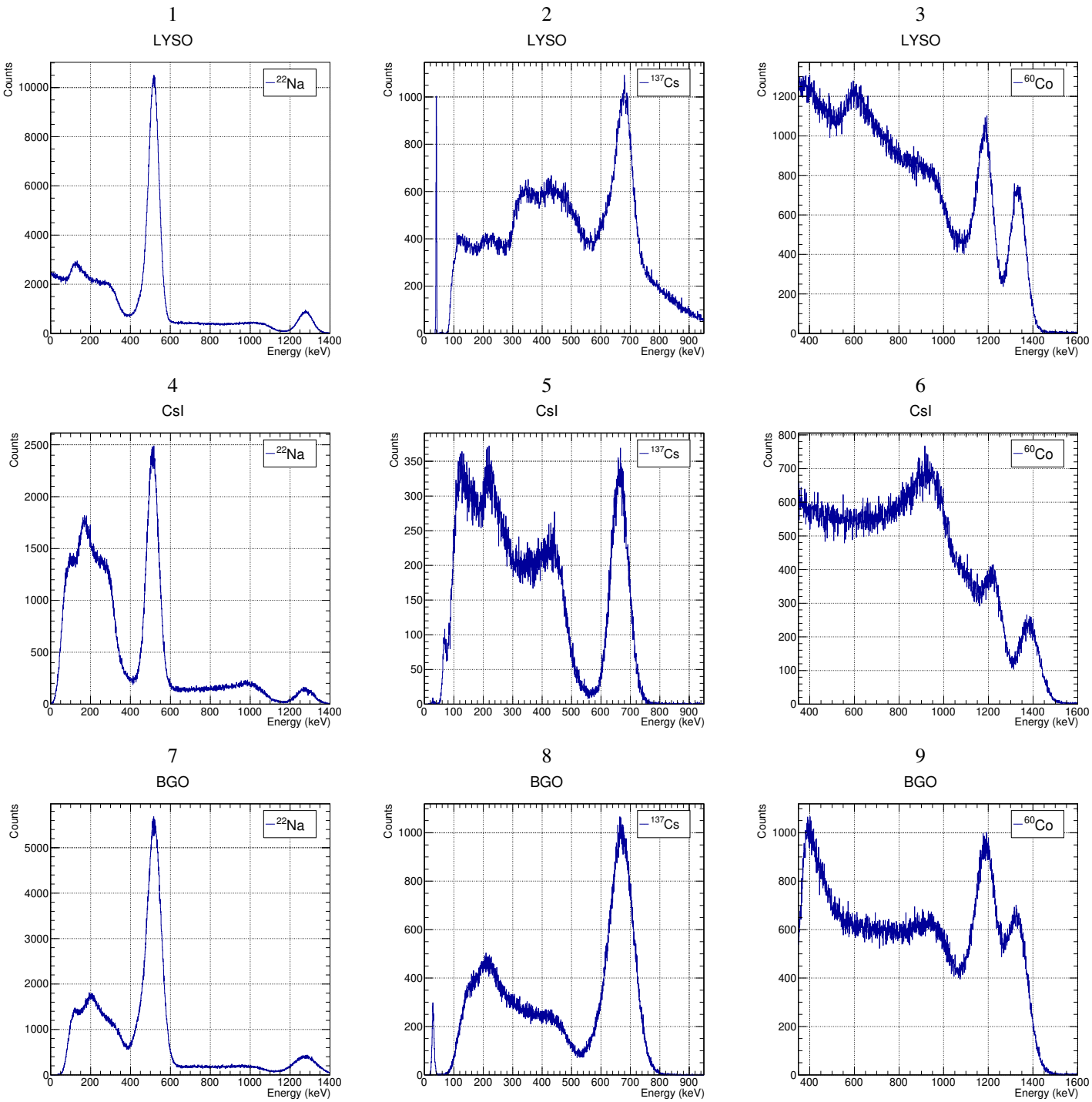

Fig. 7. Calibrated energy spectra from ^{22}Na, ^{137}Cs, and ^{60}Co γ radioactive sources (from left to right) measured with LYSO, CsI(Tl), and BGO crystals (from top to bottom) coupled with single 6×6 mm^2 SiPMs and acquired with the A5202 board. The prominent Compton background, especially in the case of CsI(Tl), is due to the reduced dimensions of the crystals; characteristic peaks are clearly visible for all the sources and for all the detectors.

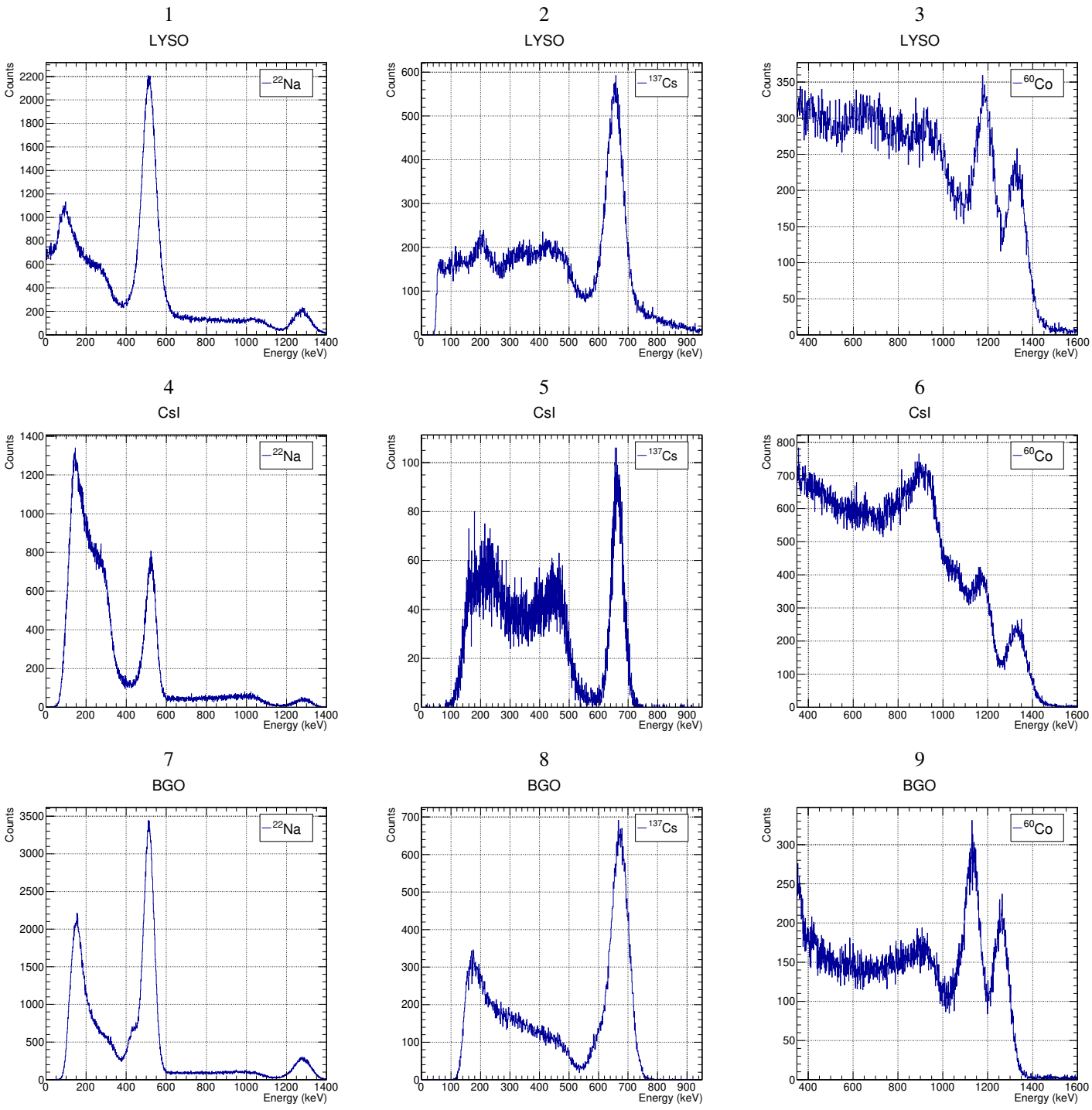

Fig. 8. Calibrated energy spectra from ^{22}Na, ^{137}Cs, and ^{60}Co γ radioactive sources (from left to right) measured with LYSO, CsI(Tl), and BGO crystals (from top to bottom) coupled with single 6×6 mm^2 SiPMs and acquired with the DT5720A board. The prominent Compton background, especially in the case of CsI(Tl), is due to the reduced dimensions of the crystals; the characteristic peaks are clearly visible for all the sources and for all the detectors.

REFERENCES

[1] "UM7945 - FERS-5200 A5202-DT5202 User Manual", CAEN SpA, Viareggio(LU), Italy, 2021. [Online] Available: www.caen.it/products/a5202. Accessed on February, 2021.

[2] "Citiroc 1A Scientific instrumentation SiPM read-out chip Data Sheet", Weeroc, Villebon-sur-Yvette, France, 2021. [Online] Available: www.weeroc.com/en/products/citiroc-1. Accessed on February, 2021.

[3] "MPPC S13360-6050CS Data Sheet", Hamamatsu, Shizuoka, Giappone, 2016. [Online] Available: www.hamamatsu.com/eu/en/product/type/S13360-6050CS/index.html. Accessed on February, 2021.

[4] V. Arosio, M. Caccia, V. Chmill, A. Ebolese, M. Locatelli, A. Martemiyanov et al., "Development of a Silicon Photomultiplier toolkit for science and education", Journal of Instrumentation, vol. 10, no. 07, pp. C07012–C07012, jul. 2015, DOI: 10.1088/1748-0221/10/07/c07012.

[5] T. Szczesniak, M. Kapusta, M. Moszynski, M. Grodzicka, M. Szawłowski, D. Wolski et al., "MPPC Arrays in PET Detectors With LSO and BGO Scintillators", IEEE Transactions on Nuclear Science, vol. 60, no.3, pp. 1533–1540, Apr. 2013, DOI: 10.1109/TNS.2013.2251002.

[6] S. David, M. Georgiou, E. Fysikopoulos, N. Belcari, G. Loudos, "Imaging performance of silicon photomultipliers coupled to BGO and CsI:Na arrays", JINST, vol. 8, no. 12, pp. P12008, Dec. 2013, DOI: 10.1088/1748-0221/8/12/P12008.

[7] A. Ulyanov, D. Murphy, A. Fredriksen, J. Ackermann, D. Meier, N. Nelms et al., "Using the SIPHRA ASIC with an SiPM array and scintillators for gamma spectroscopy", presented at IEEE NSS MIC 2017, pp. 1–3, DOI: 10.1109/NSSMIC.2017.8532845.

[8] "UM3244 - DT5720 User Manual", CAEN SpA, Viareggio(LU), Italy, 2021. [Online] Available: ww.caen.it/products/dt5720, 2017. Accessed on February, 2021.

[9] D. Impiombato, S. Giarrusso, T. Mineo, O. Catalano, C. Gargano, G. La Rosa et al., "Characterization and performance of the ASIC (CITIROC) front-end of the ASTRI camera", in Nuclear Instruments and Methods in Physics Research Section A: Accelerators, Spectrometers, Detectors and Associated Equipment, vol. 794, no. 794, pp. 185–192, 2015, DOI: https://doi.org/10.1016/j.nima.2015.05.028.

[10] D. Kyratzis, F. Alemanno, C. Altomare, F. C. T. Barbato, P. Bernardini, P. W. Cattaneo et al., "The Plastic Scintillator Detector of the HERD space mission", Proceedings of Science, ICRC2021, Belin, Germany, 2021.

[11] C. A. Kierans, "AMEGO: exploring the extreme multimessenger universe", Space Telescopes and Instrumentation 2020: Ultraviolet to Gamma Ray, SPIE, vol. 11444, pp. 528–546, 2020, DOI: 10.1117/12.2562352.

[12] F. Barbato, A. Abba, A. Anastasio, G. Barbarino, A. Boiano, R. de Asmundis et al., "The Crystal Eye X and gamma ray detector for space missions", Proceedings of 37th International Cosmic Ray Conference — PoS(ICRC2021), vol. 395, pp. 581, 2021, DOI: 10.22323/1.395.0581.

[13] J. Allison, P. Antkowiak, N. Bellam, F. Castro, L. Chen, P. Correia et al., "Wearable Positron Emission Tomography, WPET", Public deliverable for the ATTRACT Final Conference, 2020.

[14] M. Fang, S. Pani, A. Di Fulvio, "Enabling PSD-capability for a High-density Channel Imager", Abstract N-03-07, in 2021 IEEE NSS MIC, Yokohama, Japan, 2021.

[15] R. Santoro, N. Ampilogov, C. Tintori, M. Caccia, "Qualification of a Silicon Photomultiplier scalable readout system", Abstract N-09-039, in 2021 IEEE NSS MIC, Yokohama, Japan, 2021.

[16] G. E. Poma, G. Cosentino, E. Fanchini, P. Finocchiaro, P. Garosi, F. Longhitano et al., "Single Photon Spectroscopy with a Flexible Front-End and Readout System for the Radioactive Waste Monitoring", Abstract n. 359, PM2021, in 15th Pisa Meeting on Advanced Detectors, Pisa, Italy, 2022.

[17] "AN8288 - Measurement of Cosmic Ray Energy Loss in Plastic Scintillators with A5202", CAEN SpA, Viareggio(LU), Italy, 2021. [Online] Available: www.caen.it/products/a5202, 2021. Accessed on February, 2021.

[18] L. Buonanno, D. Vita, M. Carminati, C. Fiorini, "GAMMA: A 16-Channel Spectroscopic ASIC for SiPMs Readout With 84-dB Dynamic Range", IEEE Transactions on Nuclear Science, vol. 68, num. 10, pp. 2559–2572, 2021, DOI: 10.1109/TNS.2021.3107333.

[19] "MPPC array S13361-3050AE-08 Data Sheet", Hamamatsu, Shizuoka, Giappone, 2020. [Online] Available: www.hamamatsu.com/eu/en/product/type/S13361-3050AE-08/index.html. Accessed on February, 2021.

[20] "MPPC module for PET Technical Note", Hamamatsu, Shizuoka, Giappone, 2017. [Online] Available: www.hamamatsu.com/resources/pdf/ssd/pet_module_kacc9009e.pdf. Accessed on February, 2021.

[21] "A525X - Adapters for FERS-5200 Board Inputs Data Sheet", CAEN SpA, Viareggio(LU), Italy, 2021. [Online] Available: www.caen.it/products/a5202. Accessed on February, 2021.

[22] "Crystal Materials Data Sheet", Hilger, Margate, England, UK, 2017. [Online] Available: www.dynasil.com/knowledge-base/crystal-materials-index. Accessed on February, 2021.

[23] "UM7946 - Janus Software User Manual", CAEN SpA, Viareggio(LU), Italy, 2021. [Online] Available: www.caen.it/products/a5202. Accessed on February, 2021.

[24] "DS2626 - SP5600 SP5600 Power Supply and Amplification Unit Data Sheet", CAEN SpA, Viareggio(LU), Italy, 2018. [Online] Available: www.caen.it/products/sp5600c. Accessed on February, 2021.

[25] "DPP-CI for SiPM User Guide", CAEN SpA, Viareggio(LU), Italy, 2010. [Online] Available: www.caen.it/products/sp5600c. Accessed on February, 2021.

[26] "MPPC (SiPM) Linearity" [Online] Available: www.hamamatsu.com/us/en/resources/interactive-tools/mppc-sipm-linearity.html. Accessed on October, 2022.